Crystal Growth and Structure Determination of Barium Rhodates: Stepping Stones toward 2H−BaRhO$_3$

Katharine E. Stitzer,[†] Ahmed El Abed,[‡,§] Jacques Darriet,[*,‡] and
Hans-Conrad zur Loye[*,†]

*Contribution from the Department of Chemistry and Biochemistry, University of South Carolina,
Columbia, South Carolina 29208, and Institut de Chimie de la Matière Condensée de Bordeaux
(ICMCB-CNRS), 87 Avenue du Dr. Schweitzer, 33608 Pessac Cedex, France*

Received July 21, 2003; E-mail: zurloye@sc.edu

Abstract: Single crystals of two new barium rhodates were grown from a molten potassium carbonate flux. The new rhodates, Ba$_{11}$Rh$_{10}$O$_{30}$ and Ba$_{32}$Rh$_{29}$O$_{87}$, are structurally related to the 2H-hexagonal perovskite structure and are characterized by pseudo one-dimensional chains of alternating face-sharing trigonal prisms and octahedra. The structures of Ba$_{11}$Rh$_{10}$O$_{30}$ and Ba$_{32}$Rh$_{29}$O$_{87}$ were solved using the 4D superspace group approach in Jana2000. Ba$_{11}$Rh$_{10}$O$_{30}$, with a repeat of nine RhO$_6$ octahedra followed by one RhO$_6$ trigonal prism, contains the longest chain sequence of face-sharing octahedra known for this 2H-perovskite related family of oxides. A structural analysis of these two compounds revealed clear trends in metal−metal distances and octahedral heights not previously identified for this family of oxides. The application of these trends toward the structure of the all-octahedra-containing end member of the structural series, the hypothetical 2H−BaRhO$_3$, enabled a prediction of its rhodium−rhodium distance, octahedral height, and lattice parameters.

Introduction

For the past several years, there has been much interest in the preparation and investigation of a family of oxides structurally related to the 2H-hexagonal perovskite structure.[1−4] This interest is spurred on by the family's compositional flexibility, as almost every element from the periodic table has been inserted into these structures, as well as by the structural variety observed for these phases. Moreover, the ability to obtain many of these new compounds in single-crystal form has further encouraged interest in this family, as it has enabled the single-crystal X-ray diffraction analysis of these compositionally and structurally complex phases.[1,4−6] We have been exploring the synthesis of new barium rhodates belonging to this family of oxides,[1−4] the prototype of which, Sr$_4$PtO$_6$, was first prepared in 1959 by Randall and Katz[7] and forms in the K$_4$CdCl$_6$ structure type. As shown by Darriet and Subramanian,[8] and more recently by Darriet, Perez-Mato, et al.,[9] the structures of all of these oxides can be described as resulting from the hexagonal stacking of m[A$_3$O$_9$] layers with n[A$_3$A′O$_6$] layers, followed by the subsequent filling of the interstitial octahedral B sites, Figure 1. The general formula that can be derived from the stacking of such layers is A$_{3n+3m}$A′$_n$B$_{3m+n}$O$_{9m+6n}$, where n and m are integers and the cation A is an alkaline earth metal, while cations A′ and B can be any number of metals including alkali, alkaline earth, transition, main group, or rare earth metals. The structures are characterized by one-dimensional chains of face-sharing A′O$_6$ trigonal prisms and BO$_6$ octahedra along the c-axis of the hexagonal unit cell.

An equivalent expression for this family of oxides is A$_{1+x}$(A′$_x$B$_{1−x}$)O$_3$, where the composition variable $x = n/(3m + 2n)$ can take on any value between 0 and $^1/_2$.[10] Thus, a value of $x = 0$ corresponds to the compound BaNiO$_3$,[11] while a value of $x = ^1/_2$ corresponds to Sr$_4$PtO$_6$,[7] that is, the two end members of this family of oxides. The compounds can also be described as modulated composite structures, where the structure is depicted as two mutually interacting subsystems modulated along z but periodic in the xy plane.[9,10,12−14] The first subsystem (1) consists of [(A′,B)O$_3$] chains with an average c-lattice

(1) Stitzer, K. E.; Darriet, J.; zur Loye, H.-C. *Curr. Opin. Solid State Mater. Sci.* **2001**, *5*, 535−544.
(2) El Abed, A.; Gaudin, E.; Darriet, J. *Acta Crystallogr.* **2002**, *C58*, i138−i140.
(3) Davis, M. J.; Smith, M. D.; zur Loye, H.-C. *J. Solid State Chem.* **2003**, *173*, 122.
(4) El Abed, A.; Gaudin, E.; zur Loye, H.-C.; Darriet, J. *Solid State Sci.* **2003**, *5*, 59.
(5) Davis, M. J.; Smith, M. D.; Stitzer, K. E.; zur Loye, H.-C. *J. Alloys Compd.* **2003**, *351*, 95−100.
(6) El Abed, A.; Elqebbaj, S. E.; Zakhour, M.; Champeaux, M.; Perez-Mato, J. M.; Darriet, J. *J. Solid State Chem.* **2001**, *161*, 300−306.
(7) Randall, J. J.; Katz, L. *Acta Crystallogr.* **1959**, *12*, 519.
(8) Darriet, J.; Subramanian, M. A. *J. Mater. Chem.* **1995**, *5*, 543.

(9) Perez-Mato, J. M.; Zakhour-Nakhl, M.; Weill, F.; Darriet, J. *J. Mater. Chem.* **1999**, *9*, 2795.
(10) Evain, M.; Boucher, F.; Gourdon, O.; Petricek, V.; Dusek, M.; Bezdicka, P. *Chem. Mater.* **1998**, *10*, 3068−3076.
(11) Lander, J. J. *Acta Crystallogr.* **1951**, *4*, 148.
(12) Ukei, K.; Yamamoto, A.; Watanabe, Y.; Shishido, T.; Fukuda, T. *Acta Crystallogr.* **1993**, *B49*, 67.
(13) Zakhour-Nakhl, M.; Claridge, J. B.; Darriet, J.; Weill, F.; zur Loye, H.-C.; Perez-Mato, J. M. *J. Am. Chem. Soc.* **2000**, *122*, 1618.
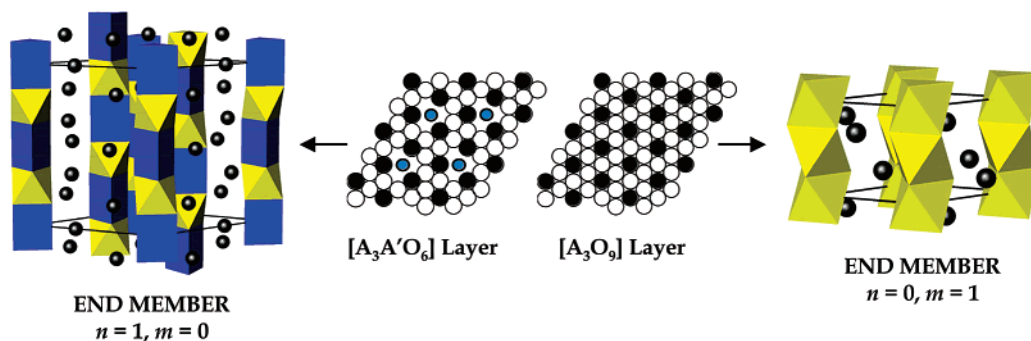(14) Zakhour-Nakhl, M.; Weill, F.; Darriet, J.; Perez-Mato, J. M. *Int. J. Inorg. Mater.* **2000**, *2*, 71.

Figure 1. Scheme for the formation of the end members, $A_3A'BO_6$ (left) and ABO_3 (right), that result from the stacking of the $[A_3A'O_6]$ and $[A_3O_9]$ layers.

parameter c_1 close to $c_{2H}/2$, and the other subsystem (2) is formed by the A cations and has a c-lattice parameter $c_2 = c_{2H}$ (c_{2H} represents the c-parameter of the ideal 2H perovskite structure). Thus, the composition of a given compound is directly related to the γ-value $= c_2*/c_1* = c_1/c_2$ by the relation $\gamma = (1 + x)/2$.[9,10] The structure of a compound $A_{1+x}(A'_xB_{1-x})O_3$ is commensurate if x is a rational value and can be matched exactly to a fraction p/k but is formally incommensurate only if x has an irrational value. A detailed explanation of the composite structure approach and its description using the superspace formalism can be found in the following papers and references therein: refs 15−19.

Numerous examples of the $n = 1$, $m = 0$ ($x = {}^1/_2$) member of the 2H perovskite related family have been synthesized including Sr_4PtO_6,[7] Sr_3NaSbO_6,[20] Ca_3NiMnO_6,[21] Sr_3NiPtO_6,[22] Ca_3NiIrO_6,[23] Ca_3CuRhO_6,[3] Sr_3ScNiO_6,[24] Sr_3NiPbO_6,[25] Sr_3NiRhO_6,[26] and Ca_3CuIrO_6.[27] The compounds of this family can be effectively classified by the ratio of trigonal prisms (A′ cations) to octahedra (B cations), $N_{prisms}/N_{octahedra}$, which can also be extracted from the $A_{1+x}(A'_xB_{1-x})O_3$ formalism as $N_{prisms}/N_{octahedra} = x/(1 - x)$. Thus, the $n = 1$, $m = 0$ ($x = {}^1/_2$) member has a ${}^1/_1 = 1$ ratio of octahedra to trigonal prisms in the polyhedral chain and hence the largest ratio of trigonal prisms to octahedra that can be found in the sequence. Similarly, for the other end member of this family with $n = 0$, $m = 1$ ($x = 0$), where examples include $BaNiO_3$,[11] $BaMnO_3$,[28] and the hypothetical $BaRhO_3$, the $N_{prisms}/N_{octahedra}$ ratio would be ${}^0/_1 = 0$, indicating that the chain contains only face-sharing octahedra and no trigonal prisms. Hence, the family can be thought of as a continuum of structures with ever-changing values of $N_{prisms}/N_{octahedra}$ between the limits of 0 and 1. Structures with $N_{prisms}/N_{octahedra}$ values closer to 1 have a higher concentration of trigonal prisms, while structures with values closer to 0 have longer sequences of face-sharing octahedra.

Our group has been working on the synthesis, specifically the single-crystal growth, of compounds in the latter category, aiming at ever-longer sequences of face-sharing octahedra, approaching compositions such as $BaRhO_3$. To that end, we have synthesized $Sr_6Rh_5O_{15}$,[29,30] $Ba_8CoRh_6O_{21}$,[31] and $Ba_9Rh_8O_{24}$[32] with $N_{prisms}/N_{octahedra}$ values of ${}^1/_5$, ${}^1/_6$, and ${}^1/_7$, respectively. As can be deduced from the $N_{prisms}/N_{octahedra}$ values, the structures are listed with increasingly longer sequences of octahedra in the polyhedral chain. Of those three compounds listed, $Ba_9Rh_8O_{24}$ has the longest repeat with a sequence of seven face-sharing RhO_6 octahedra followed by one RhO_6 trigonal prism.

Others groups have also synthesized compounds with long octahedral repeats. One such example is the polycrystalline sample $Ba_{66}Co_{59}O_{177}$[33] whose polyhedra sequence consists of units of seven CoO_6 octahedra followed by one trigonal prism and units of eight CoO_6 octahedra followed by one CoO_6 trigonal prism. Another structure consisting of long octahedral repeats is $Ba_{1.1064}CoO_3$, an incommensurate compound, whose average structure is approximately that of $Ba_{10}Co_9O_{27}$.[6] This average structure consists of a polyhedra chain repeat of eight CoO_6 octahedra followed by one trigonal prism. Finally, another interesting compound is the structurally related orthorhombic $Ba_{12}Co_{11}O_{33}$,[34] with a repeat of 10 CoO_6 octahedra followed by one CoO_6 trigonal prism.

Although many compounds in the 2H-hexagonal related family exist, it has been difficult to recognize structural trends such as bond lengths, polyhedral height, metal−metal distances, etc. among this family due to the lack of crystallographically well-characterized structures having sufficiently long octahedral repeats. We succeeded in synthesizing and structurally characterizing two such new compounds, $Ba_{11}Rh_{10}O_{30}$ and $Ba_{32}Rh_{29}O_{87}$, that have long uninterrupted octahedra chain segments. As a result, for the first time, several trends of octahedral heights, height distributions (ratio between the trigonal prism and octahedral height), structural distortions, and structural compensations imposed by the stacking of layers to enable the metals to achieve an optimum coordination environment have become apparent within these new structures. In the limit, as the octahedral repeats become infinite, the expected structure in this

(15) van Smaalen, S. *Phys. Rev. B* **1991**, *43*, 11330.
(16) Janner, A.; Janssen, T. *Acta Crystallogr.* **1980**, *A36*, 399.
(17) Janner, A.; Janssen, T. *Acta Crystallogr.* **1980**, *A36*, 408.
(18) Perez-Mato, J. M.; Madariaga, G.; Zuñiga, F. J.; Garcia Arribas, A. *Acta Crystallogr.* **1987**, *A43*, 216.
(19) van Smaalen, S. *Cryst. Rev.* **1995**, *4*, 79.
(20) Battle, P. D.; Hartwell, S. J.; Moore, C. A. *Inorg. Chem.* **2001**, *40*, 1716.
(21) Bazuev, G. V.; Zubkov, V. G.; Berger, I. F.; Arbuzova, T. I. *Solid State Sci.* **1999**, *1*, 365.
(22) Nguyen, T. N.; Giaquinta, D. M.; zur Loye, H.-C. *Chem. Mater.* **1994**, *6*, 1642.
(23) Claridge, J. B.; Layland, R. C.; Adams, R. D.; zur Loye, H.-C. *Z. Anorg. Allg. Chem.* **1997**, *623*, 1131.
(24) James, M.; Attfield, J. P. *Chem.-Eur. J.* **1996**, *2*, 737.
(25) Smith, M. D.; Stalick, J. K.; zur Loye, H.-C. *Chem. Mater.* **1999**, *11*, 2984.
(26) Stitzer, K. E.; Henley, W. H.; Claridge, J. B.; zur Loye, H.-C.; Layland, R. C. *J. Solid State Chem.* **2002**, *164*, 220−229.
(27) Tomaszewska, A.; Müller-Buschbaum, H. *Z. Anorg. Allg. Chem.* **1993**, *619*, 534.
(28) Cussen, E. J.; Battle, P. D. *Chem. Mater.* **2000**, *12*, 831.

(29) Stitzer, K. E.; El Abed, A.; Darriet, J.; zur Loye, H.-C. *J. Am. Chem. Soc.* **2001**, *123*, 8790.
(30) Claridge, J. B.; zur Loye, H.-C. *Chem. Mater.* **1998**, *10*, 2320.
(31) zur Loye, H.-C.; Stitzer, K. E.; Smith, M. D.; El Abed, A.; Darriet, J. *Inorg. Chem.* **2001**, *40*, 5152.
(32) Stitzer, K. E.; Smith, M. D.; Darriet, J.; zur Loye, H.-C. *Chem. Commun.* **2001**, 1680.
(33) Boulahya, K.; Parras, M.; González-Calbet, J. M. *Chem. Mater.* **2000**, *12*, 25.
(34) Darriet, J.; Elcoro, L.; El Abed, A.; Gaudin, E.; Perez-Mato, J. M. *Chem. Mater.* **2002**, *14*, 3349−3363.

series is 2H−BaRhO$_3$. While we have been unable to synthesize this compound so far, we are now in a position to make some targeted predictions about 2H−BaRhO$_3$, specifically its lattice parameters and bond lengths, using the structural trends observed in the two new compounds described in this paper. For that reason, we consider Ba$_{11}$Rh$_{10}$O$_{30}$ and Ba$_{32}$Rh$_{29}$O$_{87}$ to be stepping stones toward 2H−BaRhO$_3$.

Experimental Section

Crystal Growth. For Ba$_{11}$Rh$_{10}$O$_{30}$ and Ba$_{32}$Rh$_{29}$O$_{87}$, Rh powder (0.1544 g, 1.5 mmol; Engelhard, 99.5%), BaCO$_3$ (0.2960 g, 1.5 mmol; Alfa, 99.95%), and K$_2$CO$_3$ (6.76 g, 49 mmol; Fisher, reagent grade) were mixed thoroughly and placed in an alumina crucible. The filled crucible was covered and heated in air from room temperature to the reaction temperature of 1050 °C at 600 °C/h, held at 1050 °C for 48 h, and cooled to room temperature by turning off the furnace. The flux was removed with water, aided by the use of sonication, and the crystals were isolated manually. Both compositions were isolated from the same batch of crystals.

Data Collection. Several single crystals with compositions of Ba/Rh/O were tested, and the quality of the diffraction data (crystal quality) was assessed on the basis of the size and sharpness of the diffraction spots. The data collection was carried out on an Enraf-Nonius Kappa CCD diffractometer using Mo Kα radiation ($\lambda = 0.71069$ Å). Data processing and the refinement were performed using the Jana2000 program package.[35] An analytical absorption correction was applied, for which the shape of the crystal was determined using the video microscope of the KappaCCD instrument.

Ba$_{11}$Rh$_{10}$O$_{30}$. From the CCD diffractometer, a unit cell corresponding to $a = 10.0439(1)$ Å, $b = 10.0439(1)$ Å, $c = 51.578$ Å was determined from 98 reflections. Of these 98 reflections, the $hkl0$ and $hk0m$ reflections belonging to each of the two subsystems, [RhO$_3$] and [Ba], respectively, were identified. From the $hkl0$ reflections, the value of c_1 = 2.579 Å for the [RhO$_3$] subsystem (subsystem 1) was obtained. Likewise, the c_2 parameter was determined from the $hk0m$ reflections, where $c_2 = 4.689$ Å for the [Ba] subsystem (subsystem 2). As previously shown for these composite systems,[9,10,36] the interactions between these two subsystems generate a modulation vector **q** along the c-axis. If the [RhO$_3$] subsystem is chosen as the reference subsystem, the modulation vector component γ is expressed as $\gamma = c_1/c_2$ ($=c_2$*/c_1*). The modulation component γ therefore equals $\gamma = c_1/c_2 = 2.579/4.689 = 0.5500$. In this case, the γ value of 0.5500 corresponds exactly to the fraction 11/20, and hence the structure is commensurate. The final data were collected in the [RhO$_3$] subsystem, where $a = 10.0439$ Å, $c_1 = 2.579$ Å, for which the components of the **q** vector are (0 0 11/20). Relevant crystallographic information is compiled in Table 1, and the atomic coordinates and associated 4D parameters are presented in Tables 2−4 for Ba$_{11}$Rh$_{10}$O$_{30}$.

Ba$_{32}$Rh$_{29}$O$_{87}$. From the CCD diffractometer, a unit cell corresponding to $a = 5.8026$ Å, $b = 5.8030$ Å, $c = 4.6813$ Å with **q** = $(-^1/_3, ^2/_3, -0.1875)$ was determined from 150 reflections. Note that, in this case, the modulated cell was chosen as the unit cell used for determining the c_1 and c_2 parameters from the supercell. From these data, the c_1 and c_2 parameters were determined by indexing only those reflections belonging to each subsystem. Fifty of those reflections belonging to the [RhO$_3$] subsystem (subsystem 1) corresponded to the lattice parameters of $a = 10.0506$ Å, $b = 10.0510$ Å, $c_1 = 2.5827$ Å. Indexing 50 other reflections belonging only to the [Ba] subsystem (subsystem 2) resulted in the lattice parameters of $a = 5.8026$ Å, $b = 5.8030$ Å, $c_2 = 4.6813$ Å. The remaining 50 reflections represented true satellites, that is, those that can be indexed with l and $m \neq 0$ for $hklm$. The modulation component γ therefore equals $\gamma = c_1/c_2 = 2.5827/4.6813$

(35) Petricek, V.; Dusek, M. Institute of Physics: Praha, Czeck Republic, 2000.
(36) Gourdon, O.; Petricek, V.; Dusek, M.; Bezdicka, P.; Durovic, S.; Gyepesova, D.; Evain, M. *Acta Crystallogr.* **1999**, *B55*, 841.

Table 1. Crystal Data and Structure Refinement for Ba$_{11}$Rh$_{10}$O$_{30}$

empirical formula	Ba$_{11/10}$RhO$_3$
formula weight	302.0 g/mol
temperature	293 K
wavelength	Mo Kα ($\lambda = 0.71069$ Å)
crystal system	trigonal
superspace group	$R\bar{3}m(00\gamma)0s$
unit cell parameters	$a = 10.0439(2)$ Å
	$c_1 = 2.579(2)$ Å
	$\mathbf{q} = 11/20 \cdot c_1$*
volume	225.3(2) Å^3
Z	3
density (calculated)	6.675(5) g/cm^3
crystal size	$0.013 \times 0.004 \times 0.12$ mm^3
$h\ k\ l$ range	$-16 \leq h \leq 15, -15 \leq k \leq 16,$
	$-4 \leq l \leq 4, -5 \leq m \leq 5$
θ_{max}	35°
linear absorption coeff.	19.58 mm^{-1}
absorption correction	Gaussian
T_{min}/T_{max}	0.3058/0.7537
no. of reflections	32 361
R_{int}	0.1163
no. of independent reflections	3267
criterion for observed reflections	$I > 3.0\sigma(I)$
no. observed reflections	1063
$F(000)$	392
twin matrix (66%)	$1\ 0\ 0/0\ \bar{1}\ 0/0\ 0\ 1$
R factors	$R(F) = 3.07\%$, w$R(F^2) = 5.64\%$
main reflections (342)	$R(F) = 2.09\%$, w$R(F^2) = 4.23\%$
first-order satellites (482)	$R(F) = 4.05\%$, w$R(F^2) = 6.75\%$
second-order satellites (239)	$R(F) = 5.80\%$, w$R(F^2) = 10.77\%$
no. of refined parameters	44
weighting scheme	$w = 1/\sigma^2(I)$
diff. Fourier residues	$[-1.93, +1.67]$ e/Å^3

Table 2. Average Atomic Positions, Crenel Functions, and Anisotropic Displacement Parameters U_{ij} (Å^2) for Ba$_{11}$Rh$_{10}$O$_{30}$

atoms	x_0	y_0	z_0	$\bar{x}_4$	Δ	U_{eq} (Å^2)^a
		Subsystem [RhO$_3$]:	$R\bar{3}m(00\gamma)0s$			
Rh1	0	0	0	0	0.45	0.0092(1)
Rh2	0	0	0	$^1/_4$	0.05	0.047(2)
O	0.1518(4)	0.1518(4)	$^1/_2$	$^1/_4$	0.5	0.016(2)
		Subsystem [Ba]:	$P\bar{3}c1(001/\gamma)$			
Ba	$^1/_3$	0	$^1/_4$			0.0118(4)

	U^{11}	U^{22}	U^{33}	U^{12}	U^{13}	U^{23}
Rh1	0.0058(1)	$=U^{11}$	0.0160(2)	$=^1/_2U^{11}$	0	0
Rh2	0.010(1)	$=U^{11}$	0.123(7)	$=^1/_2U^{11}$	0	0
O	0.012(2)	$=U^{11}$	0.011(2)	$-0.006(2)$	$-0.0004(7)$	$=-U^{13}$
Ba	0.0077(6)	$=U^{11}$	0.0200(2)	$=^1/_2U^{11}$	0	0

^{a} $U_{eq} = ^1/_3\sum_i \sum_j U^{ij}a_i^*a_j^*\mathbf{a_i}\cdot\mathbf{a_j}$. The anisotropic displacement factor exponent takes the form: $-2\pi^2\sum_i \sum_j U^{ij}a_i^*a_j^*\mathbf{h_i}\cdot\mathbf{h_j}$.

= 0.5517, which corresponds exactly to the γ value of 16/29 = 0.5517; hence the structure is commensurate. The final data were collected using the cell $a = 5.8026$ Å, $b = 5.8030$ Å, $c = 4.6813$ Å, **q** = $(-^1/_3, ^2/_3, -0.1875)$ where the main reflections of one of the subsystems, in this case subsystem 2, was collected as well as the associated satellites, instead of collecting the data for the supercell.

Transformation of the data into the supercell was carried out in several steps. The first applied the following matrix to the data which changed a and b to be approximately $a\sqrt{3}$ and $b\sqrt{3}$:

$$\begin{bmatrix} 2 & -1 & 0 \\ 1 & 1 & 0 \\ 0 & 0 & 1 \end{bmatrix}$$

Also, the **q** vector was transformed to $\mathbf{q_2} = (0, 1, -0.1875)$. In the second step, the rational part $(0 -1\ 2)$ was added to the $\mathbf{q_2}$ vector, resulting in $\mathbf{q_2}' = (0, 0, 1.8125)$. Applying these transformations

Table 3. Atomic Positional and Debye Waller Factors Modulation Coefficients for $Ba_{11}Rh_{10}O_{30}$ (Only Coefficients $\neq 0$ Are Shown)[a]

Rh1 $\quad U_{z,1}^{Rh1} = -0.0611(4)$ $\qquad\qquad U_{z,3}^{Rh1} = -0.0154(5)$

$\qquad U_{U11,2}^{Rh1} = U_{U22,2}^{Rh1} = 2U_{U12,2}^{Rh1} =$
$\qquad\qquad -0.00004(16)$ $\qquad\qquad\qquad U_{U33,2}^{Rh1} = -0.0095(2)$

O $\quad U_{x,1}^{O} = U_{y,1}^{O} = 0.0097(6)$ $\qquad U_{x,2}^{O} = -U_{y,2}^{O} = -0.0069(5)$
$\quad U_{z,2}^{O} = 0.063(2)$ $\qquad\qquad U_{x,3}^{O} = -U_{y,3}^{O} = 0.0086(7)$
$\quad U_{z,3}^{O} = 0.032(2)$ $\qquad\qquad U_{x,4}^{O} = U_{y,4}^{O} = 0.0051(6)$
$\quad U_{x,5}^{O} = -U_{y,5}^{O} = 0.0081(5)$ $\quad U_{z,5}^{O} = 0.029(3)$
$\quad U_{x,6}^{O} = U_{y,6}^{O} = 0.0025(9)$ $\qquad U_{x,7}^{O} = -U_{y,7}^{O} = 0.0052(8)$
$\quad U_{z,7}^{O} = 0.013(4)$ $\qquad\qquad U_{x,8}^{O} = U_{y,8}^{O} = 0.010(2)$
$\quad U_{U11,1}^{O} = U_{U22,1}^{O} = -0.010(1)$ $\quad U_{U33,1}^{O} = 0.001(2)$
$\quad U_{U12,1}^{O} = 0.005(15)$ $\qquad\quad U_{U13,1}^{O} = -U_{U23,1}^{O} = -0.0004(10)$
$\quad U_{U11,2}^{O} = -U_{U22,2}^{O} = 0.004(2)$ $\quad U_{U13,2}^{O} = U_{U23,2}^{O} = 0.005(1)$

Ba $\quad U_{x,s1}^{Ba} = \frac{1}{2}U_{y,s1}^{Ba} = -\frac{1}{\sqrt{3}}U_{x,c1}^{Ba} = -0.00633(2)$

$\qquad U_{x,s2}^{Ba} = \frac{1}{2}U_{y,s2}^{Ba} = \frac{1}{\sqrt{3}}U_{x,c2}^{Ba} = 0.00190(3)$

$\qquad U_{z,s3}^{Ba} = -0.0022(2)$

$\qquad U_{x,s4}^{Ba} = \frac{1}{2}U_{y,s4}^{Ba} = -\frac{1}{\sqrt{3}}U_{x,c4}^{Ba} = -0.0006(2)$

$\qquad U_{x,s5}^{Ba} = \frac{1}{2}U_{y,s5}^{Ba} = \frac{1}{\sqrt{3}}U_{x,c5}^{Ba} = -0.0049(4)$

$\qquad U_{U11,s1}^{Ba} = U_{U12,s1}^{Ba} = \sqrt{3}U_{U11,c1}^{Ba} = -\frac{\sqrt{3}}{2}U_{U22,c1}^{Ba} = -\sqrt{3}U_{U12,c1}^{Ba} = 0.0029(3)$

$\qquad U_{U13,s1}^{Ba} = \sqrt{3}U_{U13,c1}^{Ba} = \frac{\sqrt{3}}{2}U_{U23,c1}^{Ba} = -0.00585(9)$

$\qquad U_{U11,s2}^{Ba} = U_{U12,s2}^{Ba} = -\sqrt{3}U_{U11,c2}^{Ba} = \frac{\sqrt{3}}{2}U_{U22,c2}^{Ba} = \sqrt{3}U_{U12,c2}^{Ba} = 0.0012(2)$

$\qquad U_{U13,s2}^{Ba} = -\sqrt{3}U_{U13,c2}^{Ba} = -\frac{\sqrt{3}}{2}U_{U23,c2}^{Ba} = -0.0032(2)$

[a] Modulation functions for a parameter λ of an atom ν defined in restricted interval (for the case of Rh1 and O) are given by: $U_\lambda^\nu(x_4) = \sum_{n=0}^{k} U_{\lambda,n}^\nu \, ortho_n^\nu(x_4)$. For Ba, the modulation functions are classically expressed as: $U_\lambda^\nu(x_4) = U_{\lambda,0}^\nu + \sum_{n=1}^{k} U_{\lambda,sn}^\nu \sin(2\pi n x_4) + \sum_{n=1}^{k} U_{\lambda,cn}^\nu \cos(2\pi n x_4)$.

generated a new unit cell with lattice parameters of $a = 10.0510$ Å, $b = 10.0510$ Å, $c_2 = 4.6813$ Å, where $c_2/c_1 = 1.8125$. The third step involved transforming these data into the supercell by multiplying c_2 by 16. In the fourth step, the new data were introduced into the model where the [RhO$_3$] subsystem was chosen as the reference system, space group $R\bar{3}m(00\gamma)0s$ with $c_1 = 2.5827$ Å. It is a commensurate case with the supercell $c_s = 74.9$ Å $= 29 \cdot c_1$ and $t = ^1/_4$, and consequently the space group of the supercell is $P321$.[9] Relevant crystallographic information is compiled in Table 5, and the atomic coordinates and associated 4D parameters are presented in Tables 6−8 for $Ba_{32}Rh_{29}O_{87}$.

Microscopy. Scanning electron micrographs of several single crystals were obtained using a Philips XL 30 ESEM instrument utilized in the environmental mode. For $Ba_{11}Rh_{10}O_{30}$ and $Ba_{32}Rh_{29}O_{87}$, EDS verified the presence of barium, rhodium, and oxygen. No other extraneous elements, such as potassium or aluminum, were detected within the detection limits of the instrument.

Discussion

Structures. Black thin hexagonal needles were grown and isolated from a carbonate melt containing Ba−Rh−O. Interestingly, two different, yet closely related, crystal compositions, $Ba_{11}Rh_{10}O_{30}$ and $Ba_{32}Rh_{29}O_{87}$, were isolated from the same

Table 4. Coefficients of the Orthogonalized Functions for $Ba_{11}Rh_{10}O_{30}$[a]

$\nu = Rh1$	B_o^{Rh1}	A_1^{Rh1}	B_1^{Rh1}	A_2^{Rh1}	B_3^{Rh1}
$ortho_0^{Rh1}$	1				
$ortho_1^{Rh1}$	0	1.498			
$ortho_2^{Rh1}$	−2.078	0	3.877		
$ortho_3^{Rh1}$	0	−3.431	0	3.363	
$ortho_4^{Rh1}$	4.343	0	−5.482	0	2.441

$\nu = Rh2$	B_o^{Rh2}	B_1^{Rh2}	A_9^{Rh2}
$ortho_0^{Rh2}$	1		
$ortho_1^{Rh2}$	0	11.054	
$ortho_2^{Rh2}$	−2.708	0	3.877

$\nu = O$	B_o^{O}	A_1^{O}	B_1^{O}	A_2^{O}	A_3^{O}	A_4^{O}	B_4^{O}	B_5^{O}	B_6^{O}
$ortho_0^{O}$	1								
$ortho_1^{O}$	−2.069	3.249							
$ortho_2^{O}$	0	0	1.414						
$ortho_3^{O}$	0	0	−2.271	2.675					
$ortho_4^{O}$	−2.187	2.785	0	0	1.953				
$ortho_5^{O}$	0	0	−2.241	1.902	0	1.845			
$ortho_6^{O}$	−7.143	9.450	0	0	5.312	0	4.180		
$ortho_7^{O}$	0	0	−6.919	6.340	0	4.528	0	3.851	
$ortho_8^{O}$	−11.086	14.690	0	0	8.171	0	5.706	0	2.493

[a] The orthogonalized functions, obtained through a Schmidt orthogonalization routine, are given by: $ortho_i^\nu(x_4) = B_0^\nu + \sum_{n=1}^{k} A_n^\nu \sin(2\pi n x_4) + \sum_{n=1}^{k} B_n^\nu \cos(2\pi n x_4)$.

Table 5. Crystal Data and Structure Refinement for $Ba_{32}Rh_{29}O_{87}$

formula	$Ba_{32/29}RhO_3$
formula weight	302.5 g/mol
temperature	293 K
wavelength	Mo Kα ($\lambda = 0.71069$ Å)
crystal system	trigonal
superspace group	$R\bar{3}m(00\gamma)0s$
unit cell parameters	$a = 10.0507(2)$ Å
	$c_1 = 2.5828(1)$ Å
	$\mathbf{q} = 16/29 \cdot c_1^*$
volume	226.0(1) Å^3
Z	3
density (calculated)	6.67 g/cm^3
crystal size	$0.01 \times 0.01 \times 0.29$ mm^3
$h\,k\,l$ range	$-16 \leq h \leq 17, -17 \leq k \leq 16,$
	$-6 \leq l \leq 6, -5 \leq m \leq 5$
θ_{max}	37°
linear absorption coeff.	19.57 mm^{-1}
absorption correction	Gaussian
T_{min}/T_{max}	0.0422/0.4311
no. of reflections	23 210
R_{int}	0.0560
no. of independent reflections	5874
criterion for observed reflections	$I > 3.0\sigma(I)$
no. observed reflections	1616
F(000)	392
R factors	$R(F) = 4.04\%$, w$R(F^2) = 9.03\%$
main reflections (583)	$R(F) = 2.57\%$, w$R(F^2) = 5.58\%$
first-order satellites (629)	$R(F) = 5.00\%$, w$R(F^2) = 9.29\%$
second-order satellites (361)	$R(F) = 8.22\%$, w$R(F^2) = 17.69\%$
third-order satellites (25)	$R(F) = 28.51\%$, w$R(F^2) = 51.29\%$
fourth-order satellites (18)	$R(F) = 30.52\%$, w$R(F^2) = 41.98\%$
no. of refined parameters	33
weighting scheme	$w = 1/\sigma^2(I)$
diff. Fourier residues	$[-2.4, +3.1]$ e/Å^3

batch of crystals, suggesting that the composition is very sensitive to the time of nucleation and growth within the melt. The needles from the Ba−Rh−O batch were no thicker than 0.01 mm and ranged in length from 0.1 to 0.4 mm.

The structure refinement for both $Ba_{11}Rh_{10}O_{30}$ and

Table 6. Average Atomic Positions, Crenel Functions, and Anisotropic Displacement Parameters U_{ij} (Å²) for $Ba_{32}Rh_{29}O_{87}$

atoms	x_0	y_0	z_0	$\hat{x}_4$	Δ	U_{eq} (Å²)^a
	Subsystem [RhO$_3$]: $R\bar{3}m(00\gamma)0s$					
Rh	0	0	0			0.0097(1)
O	0.1505(3)	0.1505(3)	$^{1}/_{2}$	$^{1}/_{4}$	0.5	0.0118(8)
	Subsystem [Ba]: $P\bar{3}c1(001/\gamma)$					
Ba	$^{1}/_{3}$	0	$^{1}/_{4}$			0.0105(3)

	U^{11}	U^{22}	U^{33}	U^{12}	U^{13}	U^{23}
Rh	0.0051(1)	$=U^{11}$	0.0187(3)	$=^{1}/_{2}U^{11}$	0	0
O	0.0096(8)	$=U^{11}$	0.013(1)	0.0025(9)	−0.0010(5)	$=-U^{13}$
Ba	0.0083(4)	$=U^{11}$	0.0150(2)	$=^{1}/_{2}U^{11}$	0	0

^{a} $U_{eq} = {}^{1}/_{3} \sum_i \sum_j U^{ij} a_i^* a_j^* \mathbf{a_i \cdot a_j}$. The anisotropic displacement factor exponent takes the form: $-2\pi^2 \sum_i \sum_j U^{ij} a_i^* a_j^* \mathbf{h_i \cdot h_j}$.

Table 7. Atomic Positional and Debye Waller Factors Modulation Coefficients for $Ba_{32}Rh_{29}O_{87}$ (Only Coefficients $\neq 0$ Are Given)^a

Rh $\quad U^{Rh}_{z,s2} = -0.0825(2)$ $\qquad U^{Rh}_{z,s4} = 0.0150(3)$

$\quad U^{Rh}_{z,s6} = -0.0066(5)$

$\quad U^{Rh}_{U11,c2} = U^{Rh}_{U22,c2} = 2U^{Rh}_{U12,c2} = -0.0008(1)$ $\quad U^{Rh}_{U33,c2} = -0.0209(4)$

$\quad U^{Rh}_{U11,c4} = U^{Rh}_{U22,c4} = 2U^{Rh}_{U12,c4} = 0.0008(2)$ $\quad U^{Rh}_{U33,c4} = 0.0109(4)$

O $\quad U^{O}_{x,1} = U^{O}_{y,1} = 0.0108(3)$ $\qquad U^{O}_{x,2} = -U^{O}_{y,2} = -0.0089(2)$

$\quad U^{O}_{z,2} = 0.056(1)$ $\qquad U^{O}_{x,3} = -U^{O}_{y,3} = 0.0103(2)$

$\quad U^{O}_{z,3} = 0.032(1)$ $\qquad U^{O}_{x,4} = U^{O}_{y,4} = 0.0054(3)$

$\quad U^{O}_{x,5} = -U^{O}_{y,5} = 0.0087(2)$ $\qquad U^{O}_{z,5} = 0.019(1)$

$\quad U^{O}_{x,6} = U^{O}_{y,6} = 0.0034(5)$

Ba $\quad U^{Ba}_{x,s1} = \frac{1}{2} U^{Ba}_{y,s1} = -\frac{1}{\sqrt{3}} U^{Ba}_{x,c1} = -0.00671(2)$

$\quad U^{Ba}_{x,s2} = \frac{1}{2} U^{Ba}_{y,s2} = \frac{1}{\sqrt{3}} U^{Ba}_{x,c2} = 0.00225(2)$

$\quad U^{Ba}_{z,s3} = -0.0023(2)$

$\quad U^{Ba}_{x,s4} = \frac{1}{2} U^{Ba}_{y,s4} = -\frac{1}{\sqrt{3}} U^{Ba}_{x,c4} = -0.0005(1)$

$\quad U^{Ba}_{x,s5} = \frac{1}{2} U^{Ba}_{y,s5} = \frac{1}{\sqrt{3}} U^{Ba}_{x,c5} = -0.0031(4)$

$\quad U^{Ba}_{U11,s1} = U^{Ba}_{U12,s1} = \sqrt{3}\, U^{Ba}_{U11,c1} = -\frac{\sqrt{3}}{2} U^{Ba}_{U22,c1} = -\sqrt{3}\, U^{Ba}_{U12,c1} = 0.0017(1)$

$\quad U^{Ba}_{U13,s1} = \sqrt{3}\, U^{Ba}_{U13,c1} = \frac{\sqrt{3}}{2} U^{Ba}_{U23,c1} = -0.00417(9)$

^{a} Modulation functions for a parameter λ of an atom ν defined in restricted interval (for the case of O) are given by: $U^\nu_\lambda(x_4) = \sum_{n=0}^k U^\nu_{\lambda,n}$ orth o$^\nu_n(x_4)$. For Rh and Ba atoms, the modulation functions are classically expressed as: $U^\nu_\lambda(x_4) = U^\nu_{\lambda,0} + \sum_{n=1}^k U^\nu_{\lambda,sn} \sin(2\pi n x_4) + \sum_{n=1}^k U^\nu_{\lambda,cn} \cos(2\pi n x_4)$.

$Ba_{32}Rh_{29}O_{87}$ utilized the $(3 + 1)D$ superspace formalism approach in the centrosymmetric space group $R\bar{3}m(00\gamma)0s$. Details of the refinement are presented in Tables 1 and 5 for $Ba_{11}Rh_{10}O_{30}$ and $Ba_{32}Rh_{29}O_{87}$, respectively. Both compounds have a modulated composite structure with two subsystems, [RhO$_3$] and [Ba], having the same a-parameters and different c-parameters. The use of the superspace formalism approach to describe this type of perovskite related compound is well established.[9,10,13,14,29,36,37] The structures were treated as commensurate modulated structures, as the γ value was a rational fraction, $\gamma = 11/20$ for $Ba_{11}Rh_{10}O_{30}$ and $\gamma = 16/29$ for $Ba_{32}Rh_{29}O_{87}$. For $Ba_{11}Rh_{10}O_{30}$ with $\gamma = 11/20$, the superspace

(37) Zakhour-Nakhl, M.; Darriet, J.; Claridge, J. B.; zur Loye, H.-C.; Perez-Mato, J. M. *Int. J. Inorg. Mater.* **2000**, *2*, 503.

Table 8. Coefficients of the Orthogonalized Functions for Oxygen in $Ba_{32}Rh_{29}O_{87}$^{a}

ortho^O_i	B^O_0	A^O_1	B^O_1	A^O_2	A^O_3	A^O_4	B^O_4
ortho$^O_0$	1						
ortho$^O_1$	−2.069	3.249					
ortho$^O_2$	0	0	1.414				
ortho$^O_3$	0	0	−2.271	2.675			
orth o$^O_4$	−2.187	2.785	0	0	1.953		
ortho$^O_5$	0	0	−2.241	1.902	0	1.845	
ortho$^O_6$	−7.143	9.450	0	0	5.312	0	4.180

^{a} The orthogonalized functions, obtained through a Schmidt orthogonalization routine, are given by: ortho$^\nu_i(x_4) = B^\nu_0 + \sum_{n=1}^k A^\nu_n \sin(2\pi n x_4) + \sum_{n=1}^k B^\nu_n \cos(2\pi n x_4)$.

group $R\bar{3}m(00\gamma)0s$ gives rise to two possible 3D space groups ($P\bar{3}c$ and $P3c$) depending on the t-phase section ($t = 0$ or $1/6k$ and t arbitrary, respectively). In this case, the t-phase of 0 was chosen for the structure refinement, which has the corresponding 3D space group $P\bar{3}c$. For $Ba_{32}Rh_{29}O_{87}$ with $\gamma = 16/29$, the 3D space groups generated are $P\bar{3}$, $P32$, and $P3$ for t-phase sections of $t = 0$, $^1/_4$, and t arbitrary, respectively. In this case, the t-phase of $^1/_4$ was chosen for the structure refinement with the corresponding 3D space group $P32$.

For $Ba_{11}Rh_{10}O_{30}$, a Crenel function[38,39] defined by its center ($\hat{x}_4$) and its width (Δ) was used for the description of the atomic positions of oxygen and rhodium atoms, in both the trigonal prismatic and the octahedral coordination sites. Subsystem 1, [RhO$_3$], was chosen as the reference subsystem for the system. The barium atoms were described along all of x_4 using a Fourier series to model the atomic modulation functions (AMFs). Note that only one independent position of the Ba atom was needed to describe the two types of Ba atoms belonging to the [Ba$_3$O$_9$] and [Ba$_3$RhO$_6$] layers. The superspace group of subsystem 2 [Ba] is $P\bar{3}c1(001/\gamma)$. In the case of $Ba_{32}Rh_{29}O_{87}$, a Crenel function was used to describe the oxygen atoms, while the rhodium and barium atoms were described using a Fourier series. The [RhO$_3$] subsystem 1 was again chosen as the reference subsystem.

For both $Ba_{11}Rh_{10}O_{30}$ and $Ba_{32}Rh_{29}O_{87}$, the structure solutions were begun with the refinement of the atomic positions, along with the corresponding isotropic displacement parameters. Subsequently, higher order displacive Fourier amplitude waves (2 for Rh1, 1 for Rh2, 4 for O, and 5 for Ba in $Ba_{11}Rh_{10}O_{30}$; 6 for Rh, 3 for oxygen, 5 for Ba in $Ba_{32}Rh_{29}O_{87}$), anisotropic displacement factors for all atoms, and higher order Debye−Waller factor (DWF) modulation waves (1 for Rh1, 1 for O, and 2 for Ba in $Ba_{11}Rh_{10}O_{30}$; 4 for Rh, 1 for Ba in $Ba_{32}Rh_{29}O_{87}$) were progressively introduced. Because the atomic modulation functions are not completely defined along all of the internal coordinate x_4, the higher order displacive AMFs were introduced by applying an orthogonalization procedure to the Fourier series coefficients to reduce correlations for both rhodium atoms and oxygen in $Ba_{11}Rh_{10}O_{30}$ and oxygen in $Ba_{32}Rh_{29}O_{87}$. In addition, the obverse/reverse twin law was applied to $Ba_{11}Rh_{10}O_{30}$. Final residual factors converged to $R(F) = 0.0307$ (w$R(F^2) = 0.0564$) for $Ba_{11}Rh_{10}O_{30}$ and $R(F) = 0.0404$ (w$R(F^2) = 0.0903$) for

(38) Petricek, V.; Van der Lee, A.; Evain, M. *Acta Crystallogr.* **1995**, *A51*, 529.
(39) Boucher, F.; Evain, M.; Petricek, V. *Acta Crystallogr.* **1996**, *B52*, 100.
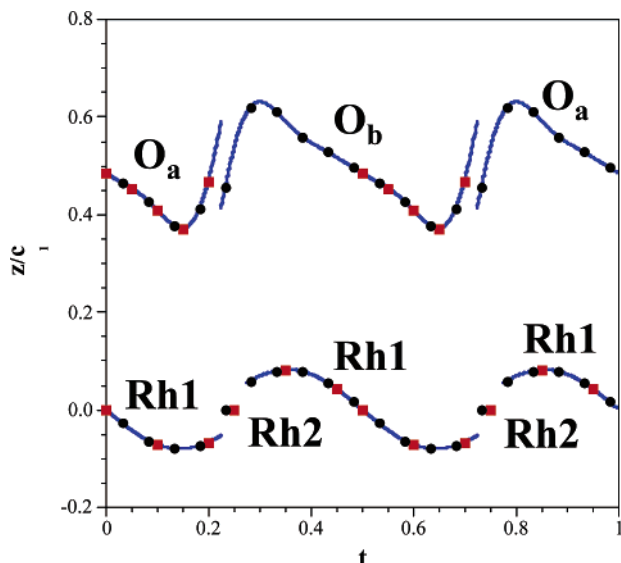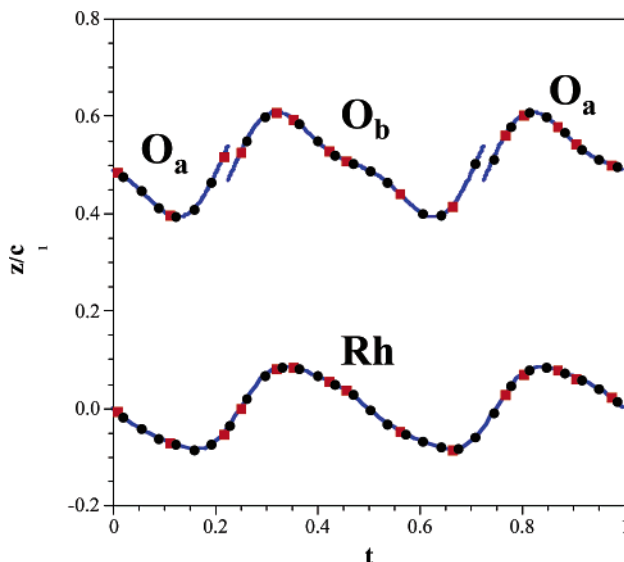
Figure 2. Variation of the fractional z-coordinate of the [RhO$_3$] subsystem versus t ($t = x_4 - \mathbf{q} \cdot \mathbf{r}_{av}$) for Ba$_{11}Rh_{10}O_{30}$. The squares and circles on the graph correspond to the commensurate z atomic coordinates in the chains located at $x \approx 0$ and $y \approx 0$ (red squares) and $x \approx \frac{1}{3}$ and $y \approx \frac{2}{3}$ (black circles).

Figure 3. Variation of the fractional z-coordinate of the [RhO$_3$] subsystem versus t ($t = x_4 - \mathbf{q} \cdot \mathbf{r}_{av}$) for Ba$_{32}Rh_{29}O_{87}$. The squares and circles on the graph correspond to the commensurate z atomic coordinates in the chains located at $x \approx 0$ and $y \approx 0$ (red squares) and $x \approx \frac{1}{3}$ and $y \approx \frac{2}{3}$ (black circles).

Ba$_{32}$Rh$_{29}$O$_{87}$. The final refinement data for both compounds are located in Tables 1−8.

For modulated structures, the atoms are described by an average position (x_0, y_0, z_0) plus an atomic modulation function (AMF) $U_r(x_4) = (U_x(x_4), U_y(x_4), U_z(x_4))$. Figures 2 and 3 are plots of the variation of the fractional z-coordinates of the atomic positions versus t ($t = x_4 - \mathbf{q} \cdot \mathbf{r}$) for the oxygen and rhodium atoms for Ba$_{11}$Rh$_{10}$O$_{30}$ and Ba$_{32}$Rh$_{29}$O$_{87}$, respectively. The squares and circles on the graphs correspond to the commensurate case and, for subsystem 1, represent the chains located at $x \approx 0$ and $y \approx 0$ (red squares) and $x \approx \frac{1}{3}$ and $y \approx \frac{2}{3}$ (black circles). As shown from the plots, the atoms are effectively modeled by the Fourier series. Note the difference between the two plots for the Rh modulation. In the case of Ba$_{11}$Rh$_{10}$O$_{30}$,

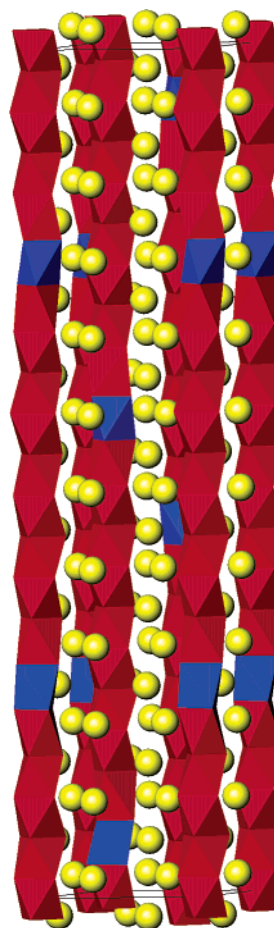**Figure 4.** Approximate [110] view of the structure of Ba$_{11}$Rh$_{10}$O$_{30}$ consisting of chains of nine RhO$_6$ octahedra followed by one RhO$_6$ trigonal prism. Blue, RhO$_6$ trigonal prism; red, RhO$_6$ octahedra; yellow spheres, Ba cations.

two Rh atoms were used in the refinement for the octahedral and trigonal prismatic sites, as can be seen from the break in the plot. In contrast, for Ba$_{32}$Rh$_{29}$O$_{87}$, the Rh position was refined using only one atomic position. The trigonal prismatic site can be grouped together with the octahedral site in Ba$_{32}$Rh$_{29}$O$_{87}$, as the width of the position is small in comparison to the width of the octahedral domain, which is effectively described by the modulation functions.

An approximate [110] view of the composite structures of Ba$_{11}$Rh$_{10}$O$_{30}$ and Ba$_{32}$Rh$_{29}$O$_{87}$ is shown in Figures 4 and 5, respectively. The structure of Ba$_{11}$Rh$_{10}$O$_{30}$ consists of a repeat of nine face-sharing RhO$_6$ octahedra followed by one RhO$_6$ trigonal prism. This is the longest consecutive sequence of octahedra known for the 2H-hexagonal perovskite related family of compounds to date, with a $N_{prisms}/N_{octahedra}$ value of 0.111. The structure of Ba$_{32}$Rh$_{29}$O$_{87}$ contains, in addition to sequences of nine RhO$_6$ octahedra, a sequence of eight RhO$_6$ octahedra followed by one RhO$_6$ trigonal prism, forming an overall repeat of 2[9 O + TP] + 1[8 O + TP]. The $N_{prisms}/N_{octahedra}$ ratio for Ba$_{32}$Rh$_{29}$O$_{87}$ is 0.115, which is slightly greater than the ratio for Ba$_{11}$Rh$_{10}$O$_{30}$, arising from the insertion of the shorter, eight RhO$_6$ octahedral unit. These structures can be thought of as stepping stones to the hypothetical 2H−BaRhO$_3$, which would contain one-dimensional chains consisting entirely of face-sharing octahedra. As there are no ambient pressure BaRhO$_3$ or SrRhO$_3$ phases of the 2H-hexagonal variant known, this flux
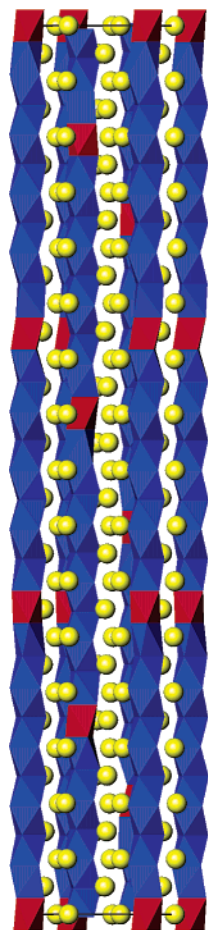
Figure 5. Approximate [110] view of the structure of $Ba_{32}Rh_{29}O_{87}$ consisting of two repeats of nine RhO_6 octahedra and one RhO_6 trigonal prism followed by one unit of eight RhO_6 octahedra and one RhO_6 trigonal prism. Red, RhO_6 trigonal prism; blue, RhO_6 octahedra; yellow spheres, Ba cations.

Figure 6. Plot of the Rh−Rh interatomic distance as a function of placement within the polyhedral chain for $Ba_{11}Rh_{10}O_{30}$ where the blue squares represent the distance between a Rh in a trigonal prism to a Rh in an adjacent octahedra and the red circles represent the distance between a Rh in an octahedra to a Rh in an adjacent octahedra.

growth method (or perhaps high pressure approaches) may be a route to successfully obtaining this compound or, at least, new compounds with still longer repeats, that is, lower $N_{prisms}/N_{octahedra}$ values.

At first glance, the compositions $Ba_{11}Rh_{10}O_{30}$ and $Ba_{32}Rh_{29}O_{87}$ might appear to be quite different; however, structurally they are closely related. Specifically, for $Ba_{11}Rh_{10}O_{30}$, $x = 1/10$, while for $Ba_{32}Rh_{29}O_{87}$, $x = 3/29$, specifying a sequence of [1 TP + 9 O] ($Ba_{11}Rh_{10}O_{30}$) versus a sequence of [1 TP + 9 O + 1TP + 9 O + 1 TP + 8 O] ($Ba_{32}Rh_{29}O_{87}$). The latter sequence is simply the juxtaposition of the sequential units corresponding to $x = 1/10$, $x = 1/10$, and $x = 1/9$, where the relationship is based on the Farey tree relationship[9] such that the ratio of $n/m = (n_1 + n_2 + ...)/(m_1 + m_2 + ...)$ or $3/29 = (1 + 1 + 1)/(10 + 10 + 9)$ where TP/oct $= n/(m - n)$. One can, thus, think of this sequence as an intergrowth between two types of structural sequences, 1 TP, 9 O and 1 TP, 8 O, in a 2:1 ratio, and anticipate that many more structurally closely related intergrowths can be grown out of a carbonate flux.

It is important when we describe these structures to be aware of the limitations in our measurements. The fractions n/m generated by the Farey tree, starting with the end members $BaNiO_3$, $x = 0/1$ and Sr_4PtO_6, $x = 1/1$, can describe the sequence of trigonal prisms and octahedra for any arbitrary composition.
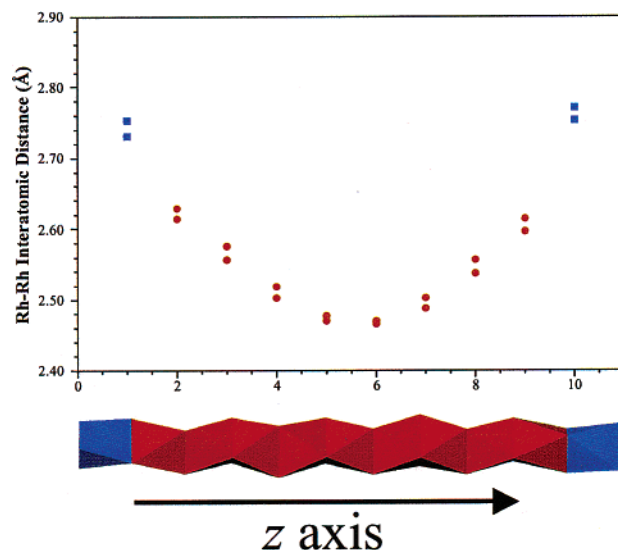
Clearly, the precision with which we determine the lattice parameters c_1 and c_2, and therefore the value of x, $(c_1/c_2) = (1 + x)/2$, ultimately limits the precision with which we can describe a structural sequence. Consequently, we must realize that all composite structures are commensurate within experimental error if sufficiently large integers n, m, are selected to "match" the value of x. We cannot, of course, exclude the possible existence of further intergrowths having a significantly longer repeat, for example, 3/29 versus 30/289, where one additional octahedron would be missing every 260 octahedra in the sequence. The modeling of such longer sequences would require greater precision in the data collection than is currently feasible. Even if it were possible, one would have to question the effect such a missing octahedron would have on the physical properties and how such a "defect" would compare to, for example, stacking fault defects known to exist in most every structure.

The Rh−O distances range from 1.9 to 2.12 Å in $Ba_{11}Rh_{10}O_{30}$ and 1.94−2.08 Å in $Ba_{32}Rh_{29}O_{87}$ and are consistent with those found in related rhodium-containing structures.[29] Upon examination of the Rh−Rh distances along the polyhedral chain, however, it was noted that there exists an unexpectedly wide range of distances, 2.47−2.75 Å in $Ba_{11}Rh_{10}O_{30}$ and 2.47−2.79 Å in $Ba_{32}Rh_{29}O_{87}$. These Rh−Rh distances are plotted in Figures 6 and 7 as a function of location within the polyhedral repeat for $Ba_{11}Rh_{10}O_{30}$ and $Ba_{32}Rh_{29}O_{87}$, respectively. As can be noted from the plot, the distances are longest for the Rh in the trigonal prismatic site at 2.75 or 2.79 Å and shortest, measuring 2.47 Å, for the Rh atom in the octahedron located in the chain halfway between two trigonal prisms. Between these two extremes, the distances follow a "V"-shaped pattern, gradually elongating to the longest Rh−Rh distance and then contracting to the shortest Rh−Rh distance. This phenomenon is not unique to these two structures, as it has been observed for $Sr_6Rh_5O_{15}$ [29] and $Ba_9Rh_8O_{24}$;[32] however, the effect is simply more striking for the longer sequences and the trend is more readily evident.

This "accordion effect" of the Rh−Rh distances within the polyhedral chain represents a structural relaxation of the trigonal
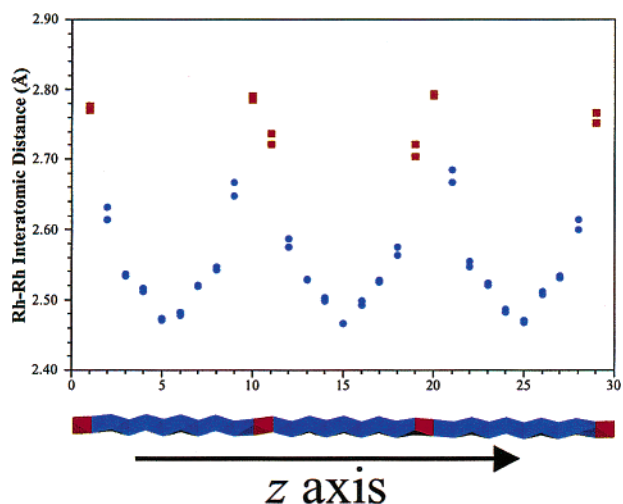
Figure 7. Plot of the Rh−Rh interatomic distance as a function of placement within the polyhedral chain for $Ba_{32}Rh_{29}O_{87}$ where the red squares represent the distance between a Rh in a trigonal prism to a Rh in an adjacent octahedra and the blue circles represent the distance between a Rh in an octahedra to a Rh in an adjacent octahedra.

prism height, caused by the unsustainable 2:1 height ratio between trigonal prisms and octahedra that results from the idealized stacking of the $[AO_3]$ and $[A_3A'O_6]$ layers. One can calculate the average layer spacing for a compound from the *c*-parameter and the corresponding number of layers for that particular composition; for example, $Ba_{11}Rh_{10}O_{30}$ has 22 layers in the supercell with a *c*-lattice parameter of 51.5780 Å corresponding to an average layer separation of 51.5780/22 or 2.34 Å. This average layer spacing coincides with the *z*-coordinate of the alkaline earth cations, [A], indicating that they indeed represent the average layer spacing. However, the positions of the oxygen atoms within the same $[AO_3]$ or $[A_3A'O_6]$ layer deviate, at times substantially, thereby increasing the height of the octahedra. This has been observed in other structural members of this family where the trigonal prism is not of ideal height in comparison to the octahedra (2:1) but rather where this height ratio has decreased, at the expense of the trigonal prism, to a ratio of at most 1.6−1.7. In fact, even this reduced ratio is only achieved in structures such as Ba_4PtO_6 [40] and Sr_4PtO_6 [7] with a repeat of one trigonal prism to one octahedron; in structures with longer octahedral sequences, this ratio decreases further and levels out at a value of only ∼1.1. As a result, the trigonal prism is much smaller than expected, almost matching the size of the octahedra, which in turn has increased in height. This suggests that the idealized octahedra are simply not large enough to accommodate the metal cations. For example, in $Ba_{11}Rh_{10}O_{30}$, the average layer distance is 2.34 Å, which should also correspond to the idealized octahedra height; however, the real structure contains no octahedra with a height of less than 2.45 Å. Therefore, it appears that the octahedra, starting from the center of the repeat sequence, have expanded to achieve a stable size for an RhO_6 octahedron by moving the oxygen atoms farther apart and, consequently, compressing the trigonal prism from an idealized height of 4.68 Å ($= 2 \times 2.34$ Å) to a measured height of only 2.75 Å.

This is readily visualized in a plot of polyhedral height as a function of position along the chain for $Ba_{11}Rh_{10}O_{30}$, shown in

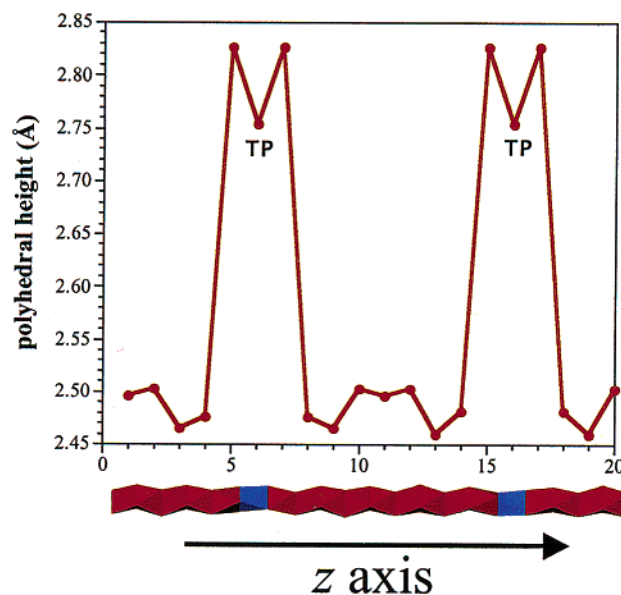(40) Wilkinson, A. P.; Cheetham, A. K. *Acta Crystallogr.* **1989**, *C45*, 1672.

Figure 8. Plot of the polyhedral height chain for $Ba_{11}Rh_{10}O_{30}$. A line has been added to guide the eye.

Figure 8. The plot reveals an almost step function height difference between the trigonal prism and its nearest octahedra neighbors and the height of the central octahedra along the chain repeat. A similar trend in the polyhedra height is observed for $Ba_{32}Rh_{29}O_{87}$. Concomitant with the "V"-shaped Rh−Rh distances within the polyhedral chain described earlier, we now find a "U"-shaped trend in polyhedral height. It appears that a height expansion starting from the center octahedra creates this accordion effect and causes a compression of the trigonal prism.

It is reasonable to expect that this accordion affect is influenced by the location of Rh(III) and Rh(IV) cations along the chain. Rhodium in $Ba_{11}Rh_{10}O_{30}$ has an average oxidation state of 3.8 and contains 8 Rh(IV) and 2 Rh(III) cations (it is unlikely that under the reaction conditions either Rh(II) or Rh(V) would be stable). It is believed that in all structures belonging to this family the larger cation in the $(A'_xB_{1-x})O_3$ chain occupies the trigonal prismatic site.[25] Hence, we would expect that one of the Rh(III) cations is located in the trigonal prism. The location of the second Rh(III) is difficult to determine by the typical methods, such as bond valence analysis; however, based on simple size arguments, we would suggest that it is located adjacent to the trigonal prismatic site, as those are the largest of the octahedral sites. It is an ongoing predicament in these oxides that unless elements with known oxidation states, such as Mg^{2+} or Zn^{2+}, are present to uniquely "fix" the oxidation states of the remaining cations, it has not been possible to assign with confidence oxidation states to specific cations in $(A'_xB_{1-x})O_3$ chains containing longer sequences of face-sharing octahedra.[32] The wide spread of metal−oxygen distances, 1.90−2.12 Å in $Ba_{11}Rh_{10}O_{30}$ and 1.94−2.08 Å in $Ba_{32}Rh_{29}O_{87}$, coupled with the at times severe distortions of the MO_6 octahedra makes it all but impossible to assign definitive oxidation states based on M−O distances alone.

Irrespective of the distribution of the Rh(III) and Rh(IV) cations along the chains, however, it is possible, from the measured RhO_6 polyhedral heights in both $Ba_{11}Rh_{10}O_{30}$ and $Ba_{32}Rh_{29}O_{87}$, to extract an approximate height requirement for an RhO_6 octahedra of about 2.47 Å. From this information, one
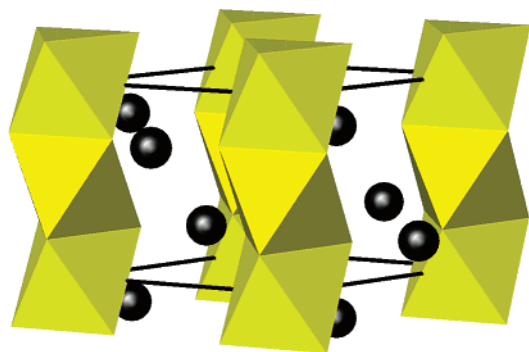
Figure 9. Structure of the proposed compound 2H−BaRhO$_3$ where the predicted lattice parameters are $a = 5.80$ Å and $c = 4.94$ Å.

can risk predicting likely lattice parameters for the 2H−BaRhO$_3$ hexagonal perovskite variant to be $a = 5.80$ Å (10.05 Å/√3) and $c = 4.94$ Å (2 × 2.47), where 10.05 Å is the *a*-parameter for both Ba$_{11}$Rh$_{10}$O$_{30}$ and Ba$_{32}$Rh$_{29}$O$_{87}$, and the *c*-parameter of the unit cell is twice the height of an octahedra. The space group is expected to be *P*6$_3$/*mmc*, and Figure 9 shows the expected structure for BaRhO$_3$.

The 2H−BaRhO$_3$ variant, so far, has managed to avoid being synthesized. Clearly, the carbonate fluxes are an excellent growth medium for Ba−Rh−O compounds, and one might anticipate that slight modifications to the conditions by which Ba$_{11}$Rh$_{10}$O$_{30}$ and Ba$_{32}$Rh$_{29}$O$_{87}$ were synthesized could lead to the isolation of 2H−BaRhO$_3$ in the future. Work in that direction is underway and will, hopefully, lead to the preparation of this elusive compound so that one can assess the accuracy of the prediction made above.

Conclusion

In summary, two new rhodium-containing oxides, structurally related to the 2H-hexagonal perovskite structure, were grown from a molten carbonate flux. The structures consist of sequences of face-sharing octahedra separated by single trigonal prisms. With a repeat of nine RhO$_6$ octahedra followed by one RhO$_6$ trigonal prism, Ba$_{11}$Rh$_{10}$O$_{30}$ is currently the compound with the longest known sequence of face-sharing octahedra in this family of oxides. Ba$_{32}$Rh$_{29}$O$_{87}$ consists of a similar sequence, but contains repeats of eight octahedra followed by one trigonal prism followed by two sequences of nine octahedra and one trigonal prism. With these long octahedra sequences, the structures begin to approach that of the 2H−BaRhO$_3$ as the octahedra are sufficiently remote from the trigonal prisms so as to be structurally isolated. Furthermore, using the structural information from these two new compounds, we were able to extract trends about octahedral height, polyhedral size ratios, structural distortions, and compensations within this family of compounds, thus resulting in structural predictions about the lattice parameters for the hypothetical 2H−BaRhO$_3$.

Supporting Information Available: Crystallographic information (CIF). This material is available free of charge via the Internet at http://pubs.acs.org.

JA0374271